ChemPubSoc Europe

DOI: 10.1002/chem.201904217

CHEMISTRY A European Journal Full Paper

Systems Chemistry |*Hot Paper*|

Programmed Recognition between Complementary Dinucleolipids To Control the Self-Assembly of Lipidic Amphiphiles

Sara Morales-Reina,[a] Chandan Giri,[a] Maxime Leclercq,[b] Sonia Vela-Gallego,[a] Isabel de la Torre,[a] José R. Castón,[c] Mathieu Surin,*[b] and Andrés de la Escosura*[a, d]

Abstract: One of the major goals in systems chemistry is to create molecular assemblies with emergent properties that are characteristic of life. An interesting approach toward this goal is based on merging different biological building blocks into synthetic systems with properties arising from the combination of their molecular components. The covalent linkage of nucleic acids (or their constituents: nucleotides, nucleosides and nucleobases) with lipids in the same hybrid molecule leads, for example, to the so-called nucleolipids. Herein, we describe nucleolipids with a very short sequence of two nucleobases per lipid, which, in combination with hydrophobic effects promoted by the lipophilic chain, allow control of the self-assembly of lipidic amphiphiles to be achieved. The present work describes a spectroscopic and microscopy study of the structural features and dynamic self-assembly of dinucleolipids that contain adenine or thymine moieties, either pure or in mixtures. This approach leads to different self-assembled nanostructures, which include spherical, rectangular and fibrillar assemblies, as a function of the sequence of nucleobases and chiral effects of the nucleolipids involved. We also show evidence that the resulting architectures can encapsulate hydrophobic molecules, revealing their potential as drug delivery vehicles or as compartments to host interesting chemistries in their interior.

Introduction

Systems chemistry represents a new approach in the molecular sciences, and encompasses a holistic view of complex chemical systems, understood as sets of diverse molecules interconnected through transformation and/or self-assembly processes.[1–3] The field of systems chemistry is thus called on to provide key insights into the resolution of major open scientific questions, such as how life could emerge from inert matter and whether it is possible to engineer artificial life-like processes and materials.[4–7] Toward this goal, it is common to study the merging of different biological building blocks into synthetic systems with properties arising from the combination of their biomolecular components.[8–10] This approach is normally based on self-organization and/or chemistries that are dynamic in nature,[11–14] and by looking closely at chiral effects of those components to reach specific morphologies.[15–17] The long-term goal of this strategy is to create chemical networks and assemblies with emergent properties that are characteristic of life.[18]

An interesting example of the aforementioned approach lies in the combination of nucleic acids (or their constituents: nucleotides, nucleosides and nucleobases) with lipids in the same hybrid molecule, leading to the so-called nucleolipids.[19,20] Whereas the main biological role of nucleic acids is to store and process genetic information, lipids are key structural elements of membranes, as boundaries that allow the compartmentalization of cellular processes. Merging the properties of nucleic acids or their molecular components with that of lipids has therefore attracted much attention in recent times,[21] mostly for the design of artificial molecular devices[22,23] and various therapeutic strategies.[24,25] Herein, we show a possible use of nucleolipids in the context of systems chemistry, to achieve control of the self-assembly of lipidic amphiphiles, either pure or in mixtures, leading to different self-assembled nano- and microstructures as a function of the sequence of nucleobases present in the nucleolipid system. Moreover, some of the structures obtained in this work can encapsulate hydrophobic molecules, revealing a potential as delivery vehicles of hydrophobic drugs or as compartments to host interesting chemistries in their interior.

A few researchers have studied the aqueous supramolecular organization of natural or synthetic nucleolipids with a single

[a] *Dr. S. Morales-Reina, Dr. C. Giri, Dr. S. Vela-Gallego, I. de la Torre, Dr. A. de la Escosura*
Department of Organic Chemistry, Universidad Autónoma de Madrid
Campus de Cantoblanco, 28049 Madrid (Spain)
E-mail: andres.delaescosura@uam.es

[b] *M. Leclercq, Dr. M. Surin*
Laboratory for Chemistry of Novel Materials
Center for Innovation in Materials and Polymers
University of Mons—UMONS, 20 Place du Parc, 7000 Mons (Belgium)
E-mail: Mathieu.surin@umons.ac.be

[c] *Dr. J. R. Castón*
Department of Structure of Macromolecules
Centro Nacional de Biotecnología/CSIC
Campus de Cantoblanco 28049 Madrid (Spain)

[d] *Dr. A. de la Escosura*
Institute for Advanced Research in Chemistry (IAdChem)
Campus de Cantoblanco, 28049 Madrid (Spain)

Supporting information and the ORCID identification number(s) for the author(s) of this article can be found under: https://doi.org/10.1002/chem.201904217.

nucleoside polar head.[26–30] This approach does not allow the self-assembly pathway to be directed through base complementarity because a single nucleobase in the polar head is not sufficient to establish adequate specificity between the nucleolipid molecules. In turn, control over self-assembly of complementary single-nucleobase monomers has been achieved in the RAFT copolymerization of methacryloyl derivatives.[31] The present article describes the first steps toward achieving this type of control over the self-assembly of lipidic amphiphiles, by designing and studying nucleolipids with two nucleobase moieties at the polar head (i.e., dinucleolipids, a term coined herein in analogy to dinucleotides). In particular, we have synthesized dinucleolipids composed of two adenine (**1 A**) or thymine (**1 T**) units, linked through amide bonds to a β-aminoalanine, the carboxylic acid group of which was previously esterified with oleyl alcohol (Figure 1 A).

Key novelties in the design of compounds **1 A** and **1 T** are the presence of two nucleobases per lipid, enriching the possible pathways of self-assembly, and the rich chemical functionality of the amino acid spacer, which enables introduction of up to three active components (i.e., two nucleobases and one lipid chain) within a three-carbon structure. Importantly, it is known that for nucleic acids such as DNA, two nucleotides are not enough to hybridize (a minimal sequence length of four nucleotides is required in high concentration of salt, e.g., 1 M NaCl).[32,33] For compounds **1 A** and **1 T**, however, hydrophobic effects promoted by the lipophilic chain cooperate with the nucleobases to favor self-assembly. A further piece of control is brought through the study of **1 A** and **1 T**, not only in the racemic form but also as enantiopure compounds (**1 A*** and **1 T***, see the stereogenic center in Figure 1 A), aimed at assessing the effect of chirality on the supramolecular organization of dinucleolipid systems by circular dichroism (CD) spectroscopy and microscopy techniques. Figure 1 B shows the strategy followed to study the aqueous self-assembly of these dinucleolipids, either alone or in 1:1 mixture. The type of assemblies obtained is determined by the nucleobase present in the dinucleolipid structure, allowing their programmed recognition when mixed. The dynamics of passing from one assembly mode to the other is also studied, as well as their capacity to incorporate hydrophobic dye molecules in the resulting assemblies.

Results and Discussion

Synthesis and spectroscopic characterization of dinucleolipid self-assemblies

Compounds **1 A** and **1 T** were prepared from β-aminoalanine, according to the synthetic pathway shown in Scheme 1. In the route to the enantiopure compounds **1 A*** and **1 T***, L-β-aminoalanine was employed as the starting material, but the experimental procedures were identical and yields were comparable to those of the racemic route. The first synthetic step consisted of an esterification of the *N*-Boc protected β-aminoalanine derivative (**2**)[34] with oleyl alcohol, mediated by 1-ethyl-3-(3-dimethylaminopropyl)carbodiimide hydrochloride (EDC). After deprotection of the amino groups in (**3**) with 4 M HCl in 1,4-dioxane, which yielded the oleyl β-aminoalanine ester derivative (**4**), an EDC-based coupling reaction with thymine-1-acetic acid (**5**) resulted in the formation of dinucleolipid **1 T**. For the synthesis of dinucleolipid **1 A**, 6-*N*-*tert*-butoxycarbonyl-9-carboxymethyladenine (**6**)[35] was used as building block in a similar coupling reaction, and so a final step of deprotection of the adenine amino group in compound **7** with trifluoroacetic acid was necessary.

The self-assembly behavior of dinucleolipids **1 A**, **1 T**, and their equimolar mixture (**1 A·1 T**), was studied in 5 mM HEPES buffer at pH 7.5. All samples were prepared by injecting small volumes of stock solutions in dimethyl sulfoxide (DMSO) (normally 1.5 or 10 mM, depending on the final target concentration) into freshly prepared HEPES buffer, ensuring that the final proportion of DMSO was $<5\%$. Under these conditions, an initial assessment of self-assembly was obtained by UV/Vis turbidity measurements, monitoring the absorbance at 400 nm (A_{400}) with dinucleolipid concentration. As none of the studied compounds present any absorption band at such a wavelength (Figure S1), this kind of measurement accounted for the scattering caused by the obtained assemblies.[36,37] In particular, Figure 2 A was assembled from three different series of concentration-dependent UV/Vis spectra (i.e., for **1 A**, **1 T** and **1 A·1 T**; see Figure S2 as an example). The scattering increased gradually with dinucleolipid concentration, showing that both **1 A** and **1 T** self-assembled in the aqueous medium, but the extent of self-assembly was much more prominent for the **1 A·1 T** mixture.

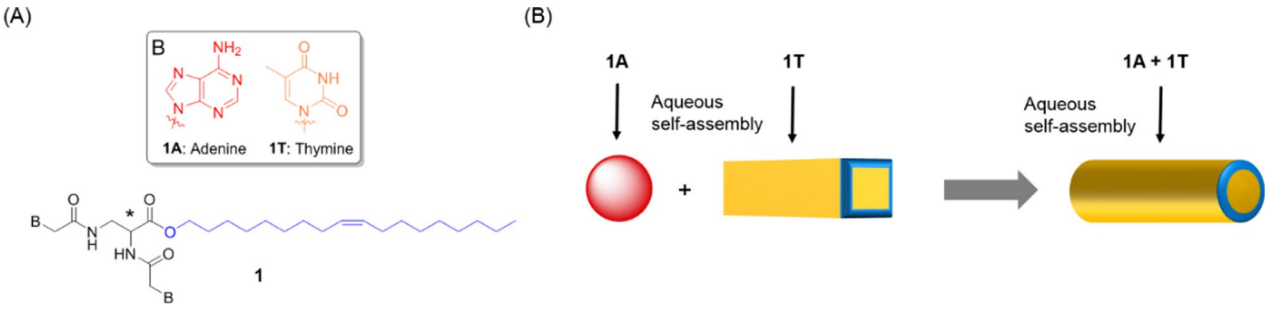

Figure 1. A) Structure of dinucleolipids **1 A** and **1 T**, presenting complementary nucleobases in each of their respective polar heads: two adenine (for **1 A**) or two thymine (for **1 T**) moieties, respectively. B) Cartoon showing the strategy for studying the types of nanostructures yielded by **1 A** (spherical assemblies) and **1 T** (crystal-like rectangular assemblies) in aqueous medium, and their transformation into a third type of structure (fibrillar assemblies) when they are mixed.

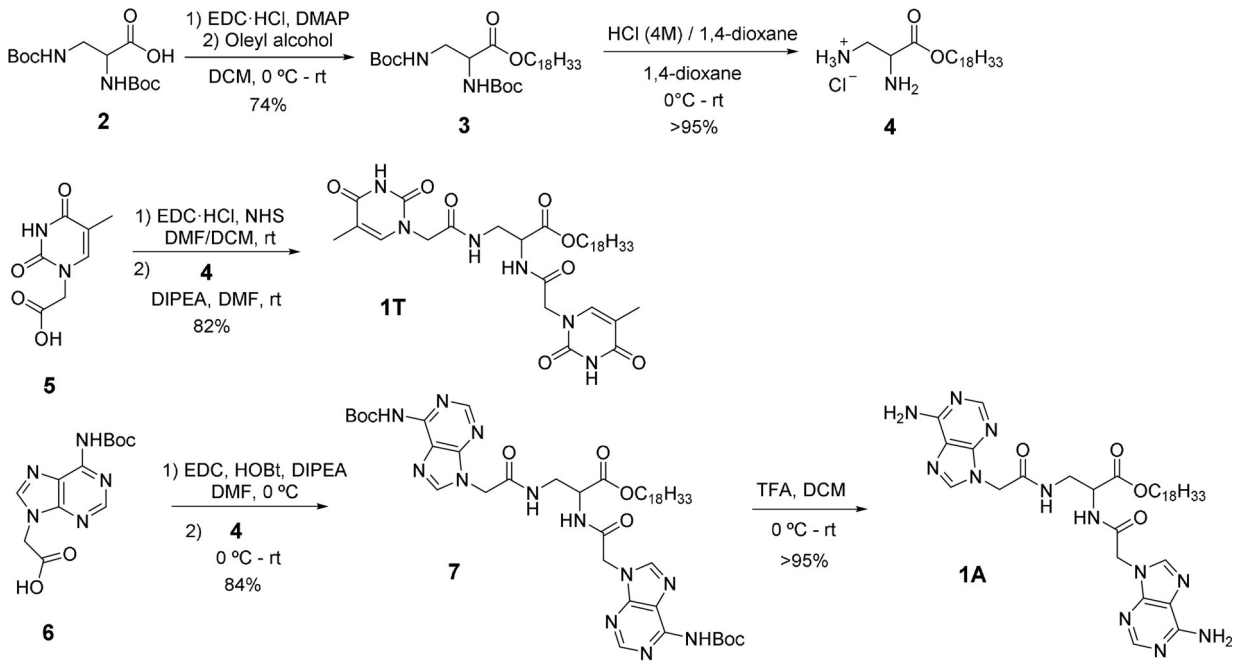

Scheme 1. Synthetic pathway for the preparation of compounds **1 A** and **1 T**.

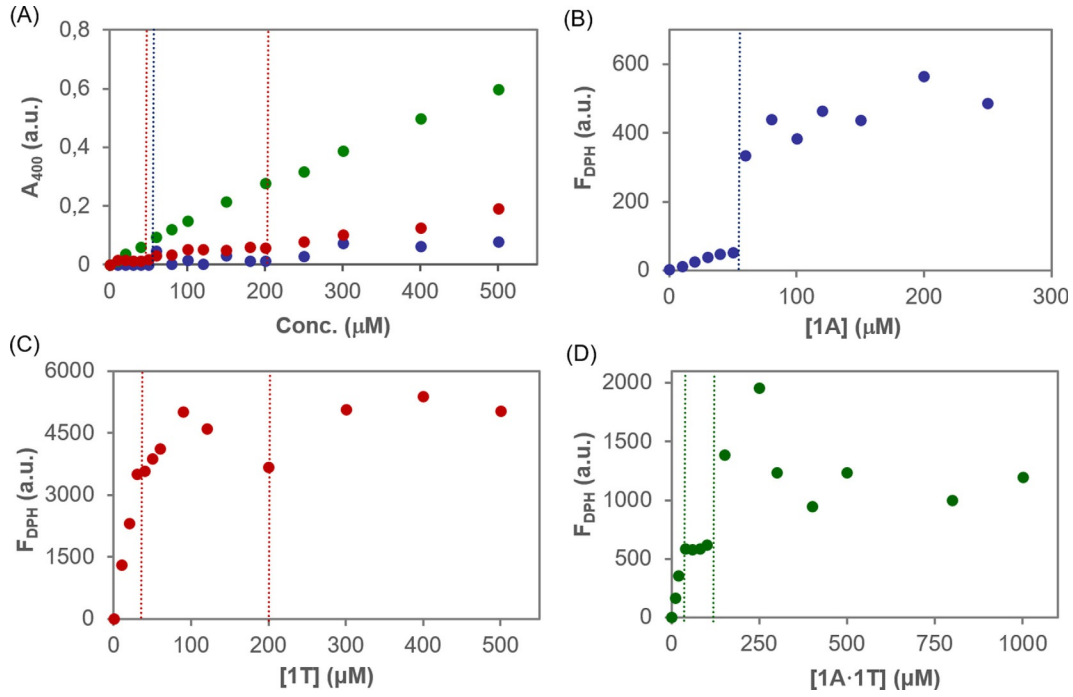

Figure 2. A) UV/Vis turbidity profiles of compounds **1 A** (blue), **1 T** (red) and the mixture **1 A·1 T** (green) versus concentration, showing scattering at 400 nm due to self-assembly in aqueous medium. Plots of the emission of the fluorescent probe DPH at 428 nm ($\lambda_{exc.}$ = 355 nm) upon adding increasing concentrations of: B) **1 A**, C) **1 T**, and D) the mixture **1 A·1 T**. The fluorescence plots were performed at 37 °C, to ensure a reasonable initial solubility of the DPH probe.

A closer inspection of the obtained turbidity profiles revealed differences in the behavior of the studied amphiphilic systems. Dinucleolipid **1 A**, for example, did not present any scattering at 400 nm until its concentration was above ca. 50 μM (Figure 2 A, blue data, blue dashed line), indicating that the adenine moieties do not induce self-assembly at low concentrations. The A_{400} started increasing from there, though with very low intensity until the **1 A** concentration was above 200 μM, probably because of the low number and size of the formed assemblies at an intermediate concentration range (see below).

For dinucleolipid **1 T** on the other hand, there was scattering throughout the examined concentration range. The absorbance profile in this case presented three regions with different

slopes, with transitions between them at ca. 50 μM and ca. 200 μM (Figure 2A, red data, red dashed lines). It is known from turbidity measurements of fatty acids and other lipid assemblies that a change in slope of the absorbance profile indicates a transition between different self-assembly regimes.[36] These regimes for compound **1T** will be discussed below, in light of their TEM inspection. Finally, the interaction between **1A** and **1T** provoked an almost linear increase of turbidity with concentration (Figure 2A, green data) that was significantly steeper than for the pure compounds **1A** or **1T** alone. Although NMR spectroscopic analysis in D_2O solution did not allow us to discern the nature of the latter interaction (due to the common intense broadening of NMR peaks in aqueous medium; data not shown), complementarity in the sequence of nucleobases of both dinucleolipids must be responsible for such an intense increase in turbidity.

To further assess the self-assembly behavior of **1A**, **1T** and **1A·1T**, fluorescence assays were conducted (Figure 2B–D), by titration of the apolar fluorescent probe 1,6-diphenyl-1,3,5-hexatriene (DPH) with increasing amounts of dinucleolipid in the same assembly buffer (5 mM HEPES, pH 7.5). DPH (2.5 μM), with excitation and emission wavelengths of 355 and 428 nm, respectively, dissolves in the hydrophobic interior of aqueous assemblies, whereupon it exhibits an increase in fluorescence that points to the critical assembly concentration (cac). The titrations were performed for dinucleolipid concentrations up to 1 mM (see Figure S3 as an example); however, data are presented until either the saturation point was reached or turbidity caused too much dispersion of data. Importantly, a cac value of ca. 50–60 μM was confirmed for compound **1A** (Figure 2B), whereas compound **1T** and the mixture **1A·1T** showed self-assembly even in the most dilute samples (10 μM) (Figure 2C and D), in accordance to the observations made by UV/Vis spectroscopy. For compound **1T**, changes in the emission profile were found at similar concentrations as for the turbidity measurements (see red dashed lines in Figure 2C). In the case of **1A·1T**, in turn, saturation is reached at much lower concentration (ca. 40 μM), which confirms the more prominent intermolecular interactions in this case. Strong aggregation actually provoked a significant dispersion of data from 150 μM and turbidity that was visible to the naked eye at the highest concentrations, indicating that the mixture was approaching its limit of solubility. Interestingly, DPH emission was more pronounced when inserted into the assemblies formed by dinucleolipid **1T** than in those formed by **1A** or the **1A·1T** mixture. This effect was confirmed by carrying out similar titrations with another fluorescent probe, coumarin 155 (C155), giving rise to a similar behavior (Figure S4), which is probably related to the internal structure and morphology of the assemblies formed by **1T** (see below).

Dynamic studies of dinucleolipid self-assembly

An interesting aspect to be explored in relation to the different self-assembly regimes shown by dinucleolipids **1A**, **1T** and **1A·1T**, is the conversion of one type of assembly (e.g., those formed by **1A** and **1T**) into a third type as a consequence of establishing complementary interactions between them. To this end, dynamic turbidity measurements were performed on assemblies arising from sequential combination of low-scattering **1A** and **1T** (Figure 2A, red/blue data) to obtain high-scattering assemblies (Figure 2A, green data). This kind of experiment has been widely utilized to study the matrix effect in self-reproducing vesicles, consisting of monitoring the increasing scattering by vesicles that grow and divide upon addition of low-scattering fatty acid micelles.[38] Figure 3 shows a representative example in which assemblies of compound **1A** (100 μM) were injected into a solution of assemblies of compound **1T** (100 μM), both in the same HEPES assembly buffering conditions (see above).

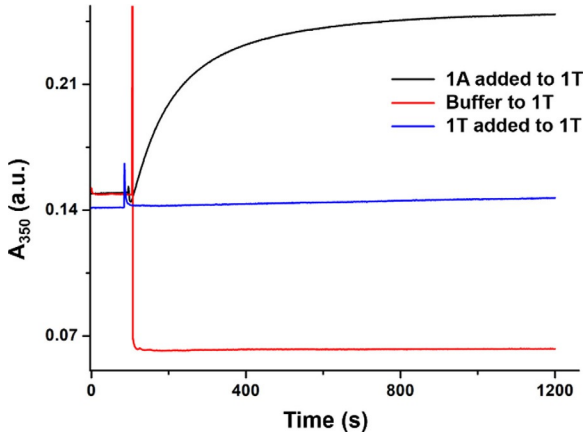

Figure 3. Dynamic turbidity experiments in which scattering at 350 nm was monitored over time, showing the transformation of low-scattering assemblies formed by **1T** into different types of high-scattering assemblies when they are mixed.

The addition of **1A** was performed directly into the UV/Vis cuvette where the absorbance of **1T** at 350 nm was being monitored in situ over time. This wavelength was chosen instead of 400 nm to increase the scattering signal, which is inversely proportional to wavelength, thus minimizing signal fluctuations that occur due to turbulence effects when the second component solution is injected into the first one. Interestingly, signal increase began immediately after mixing and reached a plateau in less than five minutes (Figure 3, black curve), revealing the very fast dynamics of conversion from one type of assembly into the other, which actually does not permit the fitting of a kinetic constant. Control experiments, in which the added solution just contained an identical volume of buffer (Figure 3, red curve) or 100 μM of compound **1T** (blue curve), showed a more prominent signal fluctuation during the first seconds after mixing, probably due to the turbulence effects noted above. After signal stabilization, however, they led to the expected results; that is, a flat line for the latter and a dilution effect for the former. The inverse experiment, in which assemblies from compound **1T** were added to assemblies from compound **1A**, revealed a similar behavior (Figure S5), suggesting that the same final assemblies are formed from both initial stages. It is important to underline

the clear differences between previous experiments, in which the dinucleolipids were first mixed in a DMSO stock, and these dynamic studies, in which the initial dinucleolipid solutions are in buffer and already preassembled.

Structural characterization of dinucleolipid self-assemblies

The size and morphology of assemblies were studied by dynamic light scattering (DLS), transmission electron microscopy (TEM) and atomic force microscopy (AFM). DLS experiments were used to determine the hydrodynamic diameter of the assemblies formed by **1A**, **1T** and the mixture **1A·1T** at various concentrations. For compound **1A**, DLS results depended on concentration: it was impossible to obtain good correlograms below the cac, whereas particles with variable, concentration-dependent sizes in a range from 97.4±42.5 nm (at 500 μM) to 244.7±147.3 nm (at 120 μM) and good polydispersity values (PDI ≈0.17 and 0.27, respectively) were observed over that threshold (Figure 4A). This inverse relationship between size and polydispersity values with concentration is common for vesicles from both ionic and neutral surfactants[39] and, together with the found size range and microscopy observations described below, suggests the possible vesicular nature of the **1A** assemblies. Compound **1T**, in contrast, showed narrow signals in the same size range (Figure 4B); that is, from 86.0± 35.2 nm (at 500 μM) to 148.8±63.9 nm (at 10 μM), with low polydispersity values (PDI ≈0.16 and 0.18, respectively) for the whole range of concentrations at which this dinucleolipid self-assembles (from 10 μM **1T**). Concerning the **1A·1T** mixture, self-assembly led to structures of a completely different nature; these were much larger in size but also more polydisperse, with correlograms of poor quality that made DLS measurements inaccurate. This result is explained by the microscopy finding that **1A·1T** forms fibrillar assemblies (see next paragraphs), and so they are not well approached using DLS spherical fitting models.

TEM provided key insights about the different self-assembly behavior presented by the two dinucleolipids alone and their mixture (Figure 4C–F). TEM samples were prepared at different concentrations and studied on carbon-coated copper grids, which were previously hydrophilized by glow discharge. Height and phase AFM images of thin dinucleolipid deposits on mica were also recorded to contrast TEM observations (Figure S6). Importantly, spherical assemblies with an average diameter of 47±5 nm (as determined by AFM, Figure S6A) were abundant over the whole sample surface for compound **1A** (Figure 4C), provided that its concentration was above the cac. At 80 μM, the assemblies appeared very dilute and ill-defined, as if they were partially formed and agglomerated (Figure S7). At higher concentrations (e.g., 200 μM), their irregular TEM appearance is probably due to flattening during the drying phase of sample preparation, as they adhere to the grid surface and dehydrate. This conclusion is reinforced by the observation that the spherical assemblies composed of enantiopure **1A*** did not present such distortion (Figure 4D and S8), probably because the better packing of **1A*** leads to a more robust structure, which does not flatten on the TEM grid. We tentatively ascribe these spherical assemblies to vesicles. However, cryo-TEM could not be performed to obtain evidence of an internal aqueous compartment, because the limited solubility of **1A** and **1A*** does not allow the concentrations required for proper cryo-freezing to be reached. Hence, the idea of other types of solid lipid nanoparticles cannot be discarded.

The behavior of dinucleolipid **1T** was very different, as it gave rise to rectangular assemblies (Figure 4E), widespread over the grid for samples containing more than 200 μM of amphiphile. At lower concentrations (e.g., 80 μM), similar objects but shorter in length were observed, and more diluted on the grid surface (Figure S9), which we hypothesize were nuclei of the more elongated nanostructures. This finding may explain the transition from two different regimes in the self-assembly of dinucleolipid **1T**, evidenced by turbidimetry and fluores-

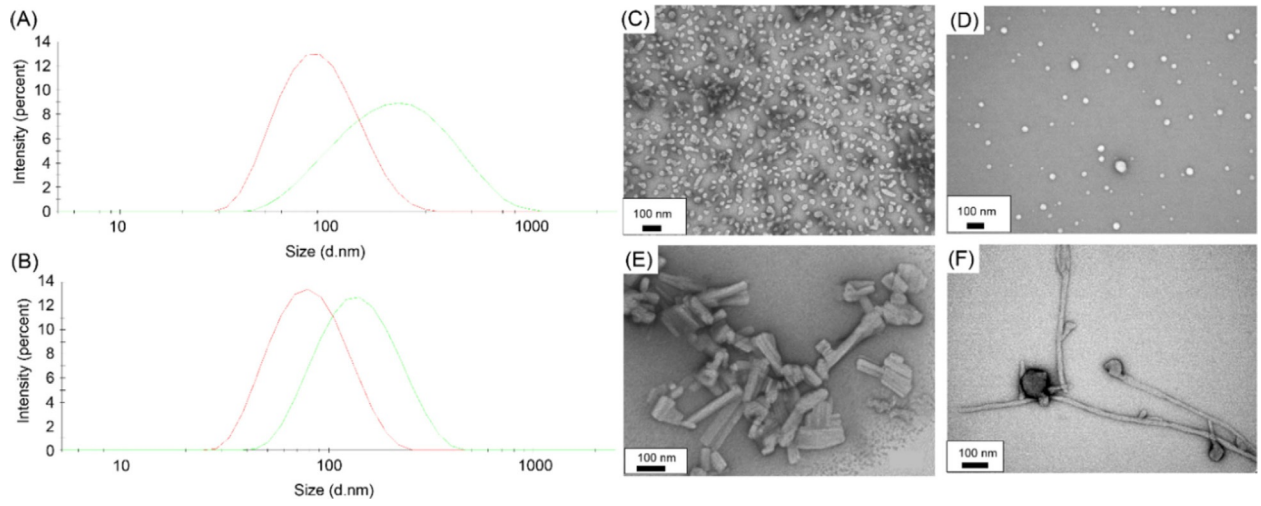

Figure 4. DLS results for compounds: A) **1A**, and B) **1T**, at low (i.e., 120 μM for **1A** and 10 μM for **1T**; green curves) and high (500 μM; red curves) concentration. Representative TEM images of the spherical, rectangular and fibrillar assemblies formed by: C) **1A**, D) **1A***, E) **1T**, and F) the mixture **1A·1T**. For the **1A·1T** mixture, it was not possible to obtain DLS data with good correlograms, due their fibrillar nature; signals corresponding to much larger and polydisperse structures were identified.

cence assays precisely at those two concentrations (see above). Interestingly, as rectangular morphologies are quite unusual for self-assembled organic nanostructures, AFM inspection was used to confirm the presence of crystal-like rectangles identical to those observed by TEM (Figure S6B). The length of these structures varied from a few hundred nm to more than 1 μm, with an average thickness of 50±7 nm. In clear contrast to the assemblies formed by pure **1 A** and **1 T**, when both dinucleolipids were mixed, TEM showed the presence of fibrillar assemblies (see Figure 4 F) with diameter values between 25 and 50 nm, and lengths in the μm scale (as determined by AFM). However, spherical and rectangular objects were also present in the samples (Figure S10). The existence of three different types of self-assembled nanostructures for racemic **1 A·1 T** was confirmed by AFM (see next section). Such imprecise control in the mixture self-assembly could be drastically improved through the use of enantiopure compounds.

Enantiopure dinucleolipid self-assemblies

To complete the spectroscopic characterization of the self-assembly behavior shown by the present dinucleolipid systems, their enantiopure versions enabled circular dichroism (CD) spectroscopy to be conducted at various concentrations and under the same conditions as for the previous spectroscopic and microscopy investigations. Importantly, whereas the racemic samples were CD silent, **1 T***, **1 A***, and **1 A·1 T*** presented CD signals in the range of 240–320 nm at concentrations of 50 and 250 μM (Figure 5 top and bottom, respectively). For most of the spectra, bisignate (+/−) CD signals were observed at both concentrations. For **1 T*** at 50 μM, three maxima were observed: a small positive peak at 295 nm, a negative peak at 282 nm, and a positive peak at 258 nm. For **1 A***, a positive peak at 287 nm and a negative peak at 256 nm were identified. At 250 μM, the triple signal of **1 T*** was somewhat modified, with a more intense positive peak at 295 nm than the large positive band around 250 nm. For **1 A*** at 250 μM, the CD signal increased more weakly with concentration compared to the CD signals of **1 T***. For the mixture of enantiopure compounds **1 A·1 T***, the bisignate CD signal shifted 10 nm to lower wavelengths when the concentration was increased from 50 to 250 μM, indicating that chiral self-assembly of the enantiopure dinucleolipids mixture was concentration-dependent.

With the aim of shedding light on the fine structure of the self-assemblies obtained from the enantiopure dinucleolipid systems, and to compare them with the racemic ones, AFM studies of 125 μM samples deposited on mica provided the most interesting insights (illustrated in Figure 6 for the mixture and in Figures S11–S13 for the rest of samples). In all cases, AFM provided additional proof of the spherical (Figure S11), rectangular (Figure S12), and fibrillar (Figure S13) assemblies formed by each dinucleolipid system, but also of the effect that enantiopurity had on their self-assembly processes. For deposits of **1 A***, for example, AFM images showed a first very thin layer of material (thickness of 0.5±0.2 nm), on top of which were small grains and some large aggregates (bright in the height image of Figure S11A). Zooming in on the small

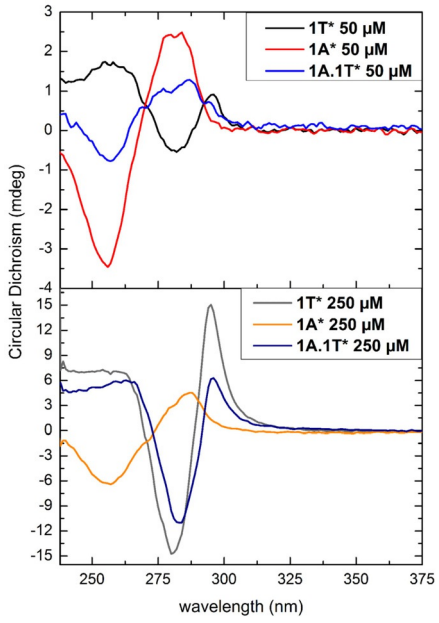

Figure 5. CD spectra of **1 T*** (black and gray lines), **1 A*** (red and orange lines) and **1 T·1 A*** (light- and dark-blue lines) at different concentrations: 50 μM (top) and 250 μM (bottom), in HEPES buffer.

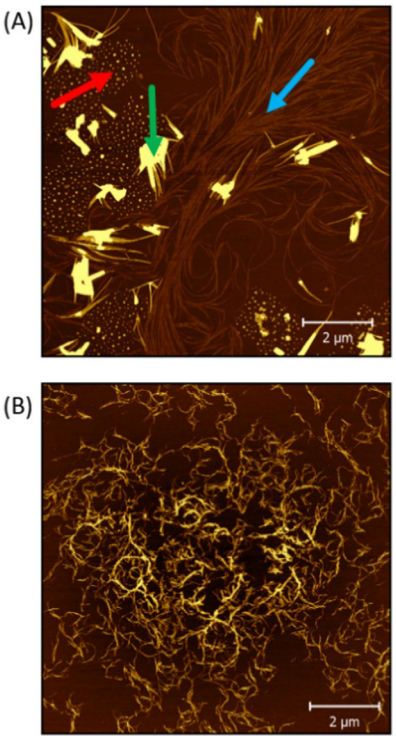

Figure 6. Tapping-mode AFM images of: A) **1 A·1 T**, and B) **1 A·1 T*** in thin deposits on mica from solutions at a concentration of 125 μM. Panel (A) is a height image, with arrows showing coexistence of spherical (red arrow), crystal-like rectangular (green arrow), and fibrillar (blue arrow) assemblies formed by racemic **1 A·1 T**, whereas panel (B) is a phase image of well-defined fibrillar assemblies formed by **1 A·1 T***. The complete set of height and phase AFM images for all samples are presented in the Supporting Information.

grains revealed their spherical structure (Figure S11B), comparable to that of other lipid vesicles studied by AFM.[40] Their average diameter was 87 ± 6 nm; almost twice that of vesicles formed by racemic **1 A**. In some areas, circumferential assemblies appeared mixed with vesicles in the phase images (Figure S11C). These very flat structures (ca. 1 nm thick), which were also observed for racemic **1 A** albeit to a lesser extent, were not visible in the TEM images, which led us to hypothesize that they could be planar tape-like deposits on the mica surface, probably as a result of evaporation effects during sample drying. For **1 T***, in turn, enantiopurity promoted the formation of straight aggregates of the same type of crystal-like rectangular assemblies previously observed for racemic **1 T**, with an average width of 60 ± 10 nm for the rectangular assemblies and a few hundred nanometer width for their aggregates (Figure S12).

The most spectacular effect of chirality on the control of self-assembly was, however, observed for the mixture of both enantiopure adenine- and thymine-containing dinucleolipids. For racemic **1 A·1 T**, the height AFM images allowed us to distinguish various coexisting morphologies (Figure 6 A, where the different assemblies are indicated with arrows), while the phase images provided further insights into their fine structure (Figure S13A), with long thin fibers arranged as dendrons, together with "crystal-like" rectangular structures and spherical assemblies (magnified image in Figure S13B) mixed with the fibers. The three types of structures match in shape and size those previously observed by TEM and AFM for **1 A**, **1 T**, and **1 A·1 T** (see above), revealing that in the racemic mixture there is a coexistence of assemblies from pure **1 A** (i.e., vesicles), pure **1 T** (i.e., rectangular structures) and mixed assemblies (the fibers). AFM images for the 1:1 mixture of **1 A·1 T*** presented, in contrast, a single type of structure, that being a well-defined network of fibrillar assemblies (Figure 6 B and S13C), in the form of short dendrites along main fibers, having an average width of 25 ± 2 nm. This result is a powerful manifestation of the importance of enantiopurity in the self-assembly properties of the studied dinucleolipids.

Dinucleolipid self-assembly models

Based on the above spectroscopic and microscopy data, together with previous models of adenine- and thymine-containing multicomponent supramolecular assemblies,[24,41–43] Figure 7 shows a schematic representation of the hypothetical structures that we propose for the assemblies formed by **1 A**, **1 T** and the mixture **1 A·1 T**. For **1 A**, turbidity measurements and fluorescence assays indicate that the interaction between adenine moieties is weak, and so self-assembly in this case must be driven mainly by the amphiphilic nature of the molecule. It is thus reasonable to propose the formation of bilayer structures (Figure 7 A) that can lead to vesicular assemblies or other lipid nanoparticles (e.g., multilayer or solid lipid nanoparticles).

The basic building block for the **1 T** rectangular assemblies, on the other hand, would be a tetramer formed through hydrogen-bonding interactions between thymine moieties (Figure S14A), as has been previously described for another multiple thymine-containing self-assembling molecule.[41] Such tetramers could then form stacks that, due to geometric constraints, would pack more closely into rectangular structures (Figure 7 B). For the mixture **1 A·1 T**, we envision two different base-pairing modes (Figure S14B and S14C), both of which could in principle lead to fibrillar assemblies, through formation of stacks of the base-paired molecular repeating units and subsequent packing of strands into fibers.[24,42–43] The scheme depicted in Figure 7 C corresponds to the first binding mode (Figure S14B), as we hypothesize it would lead to a more favorable stacking of the **1 A·1 T** dimers; although the second binding mode cannot be discarded. Importantly, these models apply to both the racemic and enantiopure systems, yet enantiopurity has a crucial effect on the degree of control that is

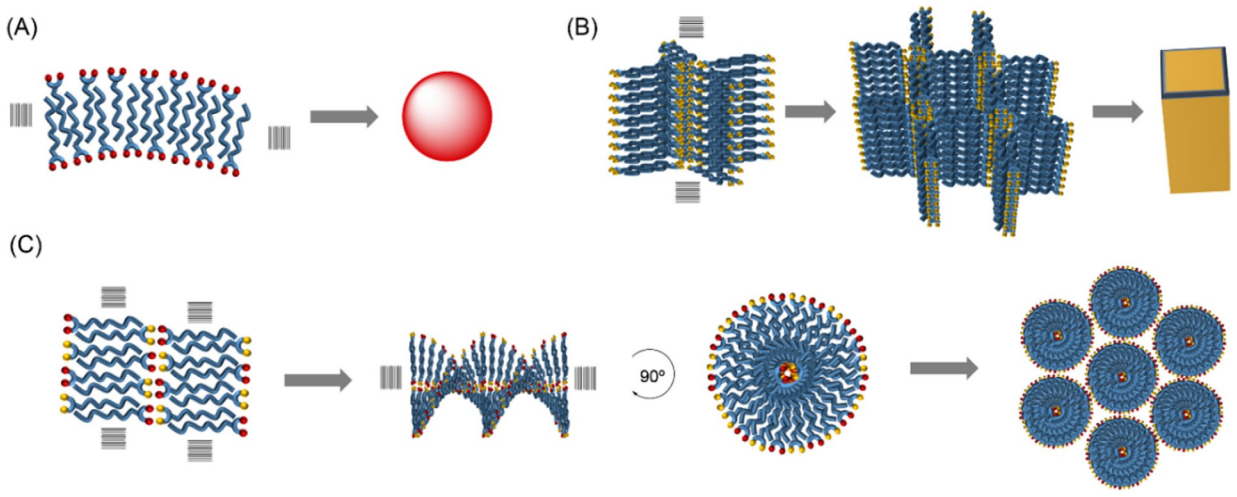

Figure 7. Schematic representation showing the hypothetical structures proposed to explain the self-assembly features of compounds: A) **1 A**, B) **1 T**, and C) the mixture **1 A·1 T**, either racemic or enantiopure. The adenine and thymine units are represented with red and yellow dots, respectively, while the long oleyl chains are represented in blue.

exerted on the self-assembly process, especially for the mixture of dinucleolipids. In particular, whereas the mixture of racemic **1A·1T** leads to a coexistence of morphologies of **1T** and of **1A** self-assemblies, together with fibrillar architectures made up of both components, the mixture of enantiopure derivatives **1A·1T*** leads to a single type of morphology, consisting of a network of thin fibers. This network of fibers is well-defined and different from the self-assemblies of the separate components, **1A*** and **1T***, as its formation is driven by programmed complementary interactions between their two constituent dinucleolipids.

Dinucleolipid self-assemblies as potential compartments

To show some potential functionality of the obtained self-assemblies, preliminary experiments based on confocal fluorescence microscopy (CFM) allowed their capacity to encapsulate hydrophobic molecules in aqueous medium to be demonstrated. Nile red was employed as the fluorescent probe because its tendency to incorporate into the hydrophobic pocket of organic assemblies in water or buffer is well known. Samples of the individual dinucleolipids (40 μM) **1A** or **1T** were imaged with Nile Red (0.5 μM) on a glass slide and, subsequently, the complementary compound **1T** or **1A** was added. Control samples containing only dye were also inspected, showing black images with no florescent objects on them. The samples were excited at $\lambda = 550$ nm and the confocal images were collected at $\lambda = 570$–650, corresponding to the orange/red emission window. Interestingly, small dots were observed in the initial images of single dinucleolipids (e.g., Figure 8A and B for **1A** and **1T**, respectively), indicating that they incorporate the hydrophobic dye. Due to the low resolution of CFM below 200 nm, it was not possible to distinguish between spherical and rectangular assemblies, as previously done by TEM and AFM. After mixing, the sample showed a completely different aspect, displaying in different regions of the glass slide the Nile Red emission along linear structures that are reminiscent of fibers (Figure 8C, corresponding to the addition of **1A** to **1T**), probably because the probe molecules tend to deposit over the formed fibrillar assemblies. These results therefore confirm the transition from one type of assembly, i.e., spherical or rectangular assemblies, into a third type of self-assembled, fibrillar nanostructure. Moreover, the three types of assemblies are able to incorporate the hydrophobic dye, suggesting that they could serve as drug nanocarriers and to host interesting chemistries. Further investigation will be undertaken in this direction.

Conclusions

In this paper we have described a series of dinucleolipid systems that allow control of the formation of and transition between different types of aqueous self-assemblies. The nucleolipids under study contain two adenine or thymine units and a hydrophobic oleyl chain directly attached to β-aminoalanine. Consequently, all the components of these nucleolipids are simple and plausibly protobiological. Moreover, they play key roles regarding the dinucleolipid self-assembly properties: the non-natural amino acid provides a high density of functional groups for grafting the other units; the oleyl chain is responsible for hydrophobic effects that contribute to self-assembly. Furthermore, having two nucleobases per nucleolipid enriches the possible pathways of self-assembly. For these reasons, the dinucleolipids **1A**, **1T**, and the mixture **1A·1T**, give rise to assemblies with completely different structural characteristics. The crystal-like rectangular assemblies formed by the thymine-containing dinucleolipid **1T** are unique from a structural point of view. Spherical lipid assemblies (e.g., micelles, vesicles, coacervates, etc.) and fibers, on the other hand, have been intensively explored in the context of systems chemistry, and the possibility to control their formation and/or interconversion based on nucleobase complementarity represents a promising approach for the development of protocell compartments[4] and replicating molecules,[44] respectively. This perspective is reinforced by a demonstration of their capacity to encapsulate hydrophobic dye molecules.

We have also provided a further piece of control of self-assembly by synthesizing enantiopure **1A*** and **1T***, which showed distinct chiroptical signals when self-assembled. Enantiopurity led to a better defined self-assembly behavior of these nucleolipids. In the future, plausible prebiotic syntheses of dinucleolipids and the potential of their assemblies as compartments or to reach non-equilibrium transient self-assembled states will be investigated. Expanding the type of obtained assemblies through small modifications of the dinucleolipid, improving their aqueous solubility to avoid the need to disperse

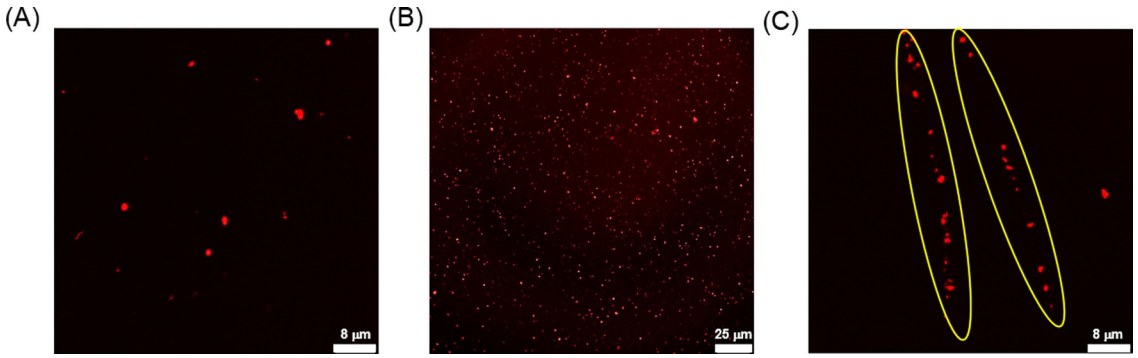

Figure 8. Confocal microscopy images of dinucleolipids A) **1A**, B) **1T**, and C) **1A·1T** at 40 μM concentration; the Nile Red probe is at 2.5 μM concentration.

them from DMSO, and further studying their structural (e.g., whether they form single- or multilayered vesicles) and dynamic behavior, are some of the open issues surrounding this new type of molecule. Moreover, possible biological targets of dinucleolipids are nucleic acids which, in addition to their interest to systems chemistry, would hold technological/biomedical potential.

Acknowledgements

Research in Madrid received support from the Spanish Ministry of Economy and Competitivity (MINECO: CTQ-2014-53673-P, CTQ-2017-89539-P, and EUIN2017-87022). This work was also supported in part by grants to JRC from MINECO (BFU2017-88736-R), and Comunidad Autónoma de Madrid (P2018/NMT-4389). A.d.l.E. and M.S. thank the interdisciplinary framework provided by the European COST Action CM1304 ("Emergence and evolution of complex chemical systems"). A.d.l.E. and C.G. acknowledge the "Programme for Post-Doctoral Talent Attraction to CEI UAM + CSIC—Intertalentum" (GA 713366). Research in Mons was supported by the Wallonia Region and the Fund for Scientific Research (FNRS, Belgium) under the grants MIS No. F.4532.16 (SHERPA) and EOS No. 30650939 (PRECISION). Confocal fluorescence microscopy was performed with the help of Sylvia Gutierrez Erlandsson, from the Advanced Light Microscopy Service of Centro Nacional de Biotecnologia (CNB). The professional editing service NB Revisions was used for technical preparation of the text prior to submission.

Conflict of interest

The authors declare no conflict of interest.

Keywords: drug delivery · fibrous structures · lipids · self-assembly · supramolecular organization

[1] E. Mattia, S. Otto, *Nat. Nanotechnol.* **2015**, *10*, 111 – 119.
[2] G. Ashkenasy, T. M. Hermans, S. Otto, A. F. Taylor, *Chem. Soc. Rev.* **2017**, *46*, 2543 – 2554.
[3] Y. S. Bai, A. Chotera, O. Taran, C. Liang, G. Ashkenasy, D. Lynn, *Chem. Soc. Rev.* **2018**, *47*, 5444 – 5456.
[4] K. Ruiz-Mirazo, C. Briones, A. de la Escosura, *Chem. Rev.* **2014**, *114*, 285 – 366.
[5] A. de la Escosura, C. Briones, K. Ruiz-Mirazo, *J. Theor. Biol.* **2015**, *381*, 11 – 22.
[6] J. D. Sutherland, *Angew. Chem. Int. Ed.* **2016**, *55*, 104 – 121; *Angew. Chem.* **2016**, *128*, 108 – 126.
[7] L. Cronin, S. I. Walker, *Science* **2016**, *352*, 1174 – 1175.
[8] M. W. Powner, B. Gerland, J. D. Sutherland, *Nature* **2009**, *459*, 239 – 242.
[9] T. Z. Jia, A. C. Fahrenbach, N. P. Kamat, K. P. Adamala, J. W. Szostak, *Nat. Chem.* **2016**, *8*, 915 – 921.
[10] H. Griesser, M. Bechthold, P. Tremmel, E. Kervio, C. Richert, *Angew. Chem. Int. Ed.* **2017**, *56*, 1224 – 1228; *Angew. Chem.* **2017**, *129*, 1244 – 1248.
[11] C. Gibard, S. Bhowmik, M. Karki, E.-K. Kim, R. Krishnamurthy, *Nat. Chem.* **2018**, *10*, 212 – 217.
[12] A. Chotera, H. Sadihov, R. Cohen-Luria, P. A. Monnard, G. Ashkenasy, *Chem. Eur. J.* **2018**, *24*, 10128 – 10135.
[13] B. V. V. S. P. Kumar, A. J. Patil, S. Mann, *Nat. Chem.* **2018**, *10*, 1154 – 1163.
[14] R. A. Black, M. C. Blosser, B. L. Stottrup, R. Tavakley, D. W. Deamer, S. L. Keller, *Proc. Natl. Acad. Sci. USA* **2013**, *110*, 13272 – 13276.
[15] M. Kumar, P. Brocorens, C. Tonnelé, D. Beljonne, M. Surin, S. J. George, *Nat. Commun.* **2014**, *5*, 5793.
[16] L. L. Đorđević, T. Marangoni, T. Miletic, J. Rubio-Magnieto, J. Mohanraj, H. Amenitsch, D. Pasini, N. Liaros, S. Couris, N. Armaroli, M. Surin, D. Bonifazi, *J. Am. Chem. Soc.* **2015**, *137*, 8150 – 8160.
[17] S. Dhiman, A. Jain, M. Kumar, S. J. George, *J. Am. Chem. Soc.* **2017**, *139*, 16568 – 16575.
[18] K. Ruiz-Mirazo, C. Briones, A. de la Escosura, *Open Biol.* **2017**, *7*, 170050.
[19] H. Rosemeyer, *Chem. Biodiversity* **2005**, *2*, 977 – 1063.
[20] A. Gissot, M. Camplo, M. W. Grinstaff, P. Barthelemy, *Org. Biomol. Chem.* **2008**, *6*, 1324 – 1333.
[21] J. Baillet, V. Desvergnes, A. Hamoud, L. Latxague, P. Barthelemy, *Adv. Mater.* **2018**, *30*, 1705078.
[22] N. Bowden, T. J. Carbeck, G. M. Whitesides, *Science* **1997**, *276*, 233 – 235.
[23] A. Petitjean, R. G. Khoury, N. Kyritsakas, J. M. Lehn, *J. Am. Chem. Soc.* **2004**, *126*, 6637 – 6647.
[24] V. Allain, C. Bourgaux, P. Couvreur, *Nucleic Acids Res.* **2012**, *40*, 1891 – 1903.
[25] K. Kowouvi, B. Alies, M. Gendrot, A. Gaubert, G. Vacher, K. Gaudin, K. Mosnier, B. Pradines, P. Barthelemy, L. Grislain, P. Millet, *RSC Adv.* **2019**, *9*, 18844 – 18852.
[26] M. Ahlers, H. Ringsdorf, H. Rosemeyer, F. Seela, *Colloid Polym. Sci.* **1990**, *268*, 132 – 142.
[27] D. Berti, P. Baglioni, S. Bonaccio, G. Barsacchi-Bo, P. L. Luisi, *J. Phys. Chem. B* **1998**, *102*, 303 – 308.
[28] L. Moreau, M. Camplo, M. Wathier, N. Taib, M. Laguerre, I. Bestel, M. W. Grinstaff, P. Barthelemy, *J. Am. Chem. Soc.* **2008**, *130*, 14454 – 14455.
[29] K. L. Gangadhara, P. Srivastava, J. Rozenski, H. P. Mattelaer, V. Leen, W. Dehaen, J. Hofkens, E. Lescrinier, P. Herdewijn, *J. Syst. Chem.* **2014**, *5*, 5.
[30] N. Taib, A. Aime, L. Moreau, M. Camplo, S. Houmadi, B. Desbat, M. Laguerre, M. W. Grinstaff, I. Bestel, P. Barthelemy, *J. Colloid Interface Sci.* **2012**, *377*, 122 – 130.
[31] Y. Kang, A. Lu, A. Ellington, M. C. Jewett, R. K. O'Reilly, *ACS Macro Lett.* **2013**, *2*, 581 – 586.
[32] M. Petersheim, D. H. Turner, *Biochemistry* **1983**, *22*, 256 – 263.
[33] J. SantaLucia, H. T. Allawi, P. A. Seneviratne, *Biochemistry* **1996**, *35*, 3555 – 3562.
[34] A. M. King, C. Salomé, J. Dinsmore, E. Salomé-Grosjean, M. D. Ryck, R. Kaminski, A. Valade, H. Kohn, *J. Med. Chem.* **2011**, *54*, 4815 – 4830.
[35] M. E. Mercurio, S. Stefano Tomassi, M. Gaglione, R. Russo, A. Chambery, S. Lama, P. Stiuso, S. Cosconati, E. Novellino, S. Di Maro, A. Messere, *J. Org. Chem.* **2016**, *81*, 11612 – 11625.
[36] A. Rendón, D. Gil Carton, J. Sot, M. Garcia-Pacios, L.-R. Montes, M. Valle, J.-L. R. Arrondo, F. M. Goñi, K. Ruiz-Mirazo, *Biophys. J.* **2012**, *102*, 278 – 286.
[37] A. Wang, C. Chan-Miller, J. W. Szostak, *Biophys. J.* **2019**, *116*, 659 – 669.
[38] A. J. Markvoort, N. Pfleger, R. Staffhorst, P. A. J. Hilberts, R. A. van Santen, J. A. Kilian, B. de Kruijff, *Biophys. J.* **2010**, *99*, 1520 – 1528.
[39] R. Bnyan, I. Khan, T. Ehtezazi, I. Saleem, S. Gordon, F. O'Neill, M. Roberts, *J. Pharm. Sci.* **2018**, *107*, 1237 – 1246.
[40] H. Schönherr, J. M. Johnson, P. Lenz, C. W. Frank, S. G. Boxer, *Langmuir* **2004**, *20*, 11600 – 11606.
[41] A. G. Slater, Y. Hu, L. Yang, S. P. Argent, W. Lewis, M. O. Blunt, N. R. Champness, *Chem. Sci.* **2015**, *6*, 1562 – 1569.
[42] L. Moreau, P. Barthelemy, M. El Maataoui, M. W. Grinstaff, *J. Am. Chem. Soc.* **2004**, *126*, 7533 – 7539.
[43] R. Iwaura, Y. Kikkawa, M. Ohnishi-Kameyama, T. Shimizu, *Org. Biomol. Chem.* **2007**, *5*, 3450 – 3455.
[44] J. M. A. Carnall, C. A. Waudby, A. M. Belenguer, M. C. A. Stuart, J. J.-P. Peyralans, S. Otto, *Science* **2010**, *327*, 1502 – 1506.

Manuscript received: September 13, 2019
Revised manuscript received: October 25, 2019
Accepted manuscript online: November 15, 2019
Version of record online: January 9, 2020